

Charge dynamics in magnetically disordered Mott insulators

Philip Bleicker^{1,*,†}, Dag-Björn Hering^{1,*,‡} and Götz S. Uhrig^{1,*,§}

Condensed Matter Theory, Technische Universität Dortmund, Otto-Hahn-Straße 4, 44221 Dortmund, Germany



(Received 21 April 2021; revised 23 December 2021; accepted 2 February 2022; published 14 February 2022)

With the aid of both a semianalytical and a numerically exact method, we investigate the charge dynamics in the vicinity of half-filling in the one- and two-dimensional t - J model derived from a Fermi-Hubbard model in the limit of large interaction U and hence small exchange coupling J . The spin degrees of freedom are taken to be disordered. So we consider the limit $0 < J \ll T \ll W$, where W is the bandwidth. We focus on evaluating the local spectral density of a single hole excitation and the charge gap that separates the upper and the lower Hubbard band. We find indications that no band edges exist if the magnetic exchange is taken into account; instead of band edges, Gaussian tails seem to appear. A discussion of the underlying physics is provided.

DOI: [10.1103/PhysRevB.105.085121](https://doi.org/10.1103/PhysRevB.105.085121)

I. INTRODUCTION

Strongly correlated fermionic systems and Mott-Hubbard physics in particular continue to represent a great challenge to theoretical treatments in spite of many decades of research [1]. Even rather clear physical questions cannot be answered in a straightforward manner. A prominent example is the motion of a single hole in a Mott insulator. This issue attracted a lot of interest soon after the discovery of high-temperature superconductivity [2] because it was noted that this phenomenon involves intimately coupled charge and spin degrees of freedom [3]. The hopping of a doped hole at half-filling scrambles the antiferromagnetic background [4], which can act as an attractive force between two holes if the second one heals the misalignments caused by the first hole [5]. Since then, a multitude of studies have appeared treating the hole motion in an ordered spin background by diagrammatic approaches [6–12]. This issue continues to be a topic of current research [13] via exact diagonalization, perturbation theory, and by time-dependent density matrix renormalization group [14]. Recently, nonequilibrium setups have become an additional focus [15]. In addition to solid-state systems, ultracold atoms in optical lattices realize fermionic Mott insulators with ordered or disordered internal degrees of freedom, e.g., a spin. The experimental possibility to detect the temporal evolution of inserted holes in real space [16,17] has rekindled the theoretical interest in quantum hole motion in various backgrounds [18–20] using analytic string theory in variational approaches, density matrix renormalization group, and matrix product states.

Even the hole motion in a *disordered* spin background is a highly nontrivial issue. At first glance, one may think that there is no order to be scrambled such that the hole can

move as freely as it does without any interaction so that the single-particle Mott gap Δ is given by $(W - U)/2$, where W is the bandwidth and U is the local Hubbard repulsion. This expectation, however, is only correct in the extreme limit $U \rightarrow \infty$ and for hole motion on self-retracing paths [4], for instance in one dimension (1D) [14,21,22]. For finite values of U in a Hubbard model, even the infinite-dimensional case yields a nontrivial value for the opening of the Mott gap computed to lie between $U_c \approx 1.11W$ [23,24] and $U_c \approx 1.19W$ [25–30]. Note that in the considered paramagnetic infinite-dimensional case, the spin background is indeed completely disordered without spin-spin correlations between different sites. Very recently, novel theoretical tools such as stochastic series expansion and special algorithms based on quantum Monte Carlo techniques [31,32] as well as novel experimental techniques for ultracold atoms [16,17] have renewed interest also in the subtle interference effects of hole motion in disordered spin backgrounds.

In 1D, the Bethe ansatz allows for an exact treatment [33] showing a Mott insulator at half-filling and zero temperature for infinitesimal interaction U . But it is also possible to consider a completely disordered spin background [34] corresponding to the situation where $J \ll T \ll U \approx W$. Here, J is the nearest-neighbor (NN) antiferromagnetic exchange coupling taking the value $4t_0^2/U$ in leading order in the NN hopping t_0 [35–40], and W is the bandwidth. Under this assumption, a Mott transition is identified to occur at $U_c = \sqrt{3}W/2 \approx 0.866W$. This finding provides an important benchmark. All these results illustrate that the hole motion is influenced by nontrivial quantum effects even for disordered spin backgrounds.

We emphasize at this stage that most previous studies on hole motion in a disordered spin background do not consider the spin dynamics, but they focus on the interference effects of the various paths of the hole [4,9,11,12]. In particular, the approach of dynamic mean-field theory (DMFT) becomes exact for an infinite coordination number, where no spin dynamics takes place [9,11,23,24,29,30]. Another special feature of DMFT for hypercubic lattices is the occurrence of

*These authors contributed equally to this work.

†philip.bleicker@tu-dortmund.de

‡dag.hering@tu-dortmund.de

§goetz.uhrig@tu-dortmund.de

Gaussian tails already in the bare density of states (DOS), which smears out tails from other physical mechanisms. In the context of hole motion without spin dynamics, one focus is the occurrence of band tails due to hopping of the hole in a ferromagnetically polarized cluster where no destructive interference occurs so that band tails may occur over the full support of the unrestricted hopping, i.e., over the full bandwidth W , but with reduced weight in the tails [4,9,11].

The aim of the present article is to study the hole motion in one and two dimensions (2D), i.e., along a chain and on a square lattice, including spin dynamics. The former case serves both as a benchmark and, due to its lower coordination number, as a system in which a larger number of processes with a larger spread is more numerically accessible than in lattices with higher coordination numbers. The latter case of a two-dimensional square lattice actually represents the most interesting case in view of experimental realizations in solid-state systems or in ultracold atom setups. We consider the generalized t - J model, which is derived from the Hubbard model [35–41] in up to second order in the hopping. We stress that in this order, the mapping of the Hubbard model to a kind of t - J model is not restricted to the magnetic exchange couplings, but naturally extends to the charge degrees of freedom, i.e., to hopping terms, hole-hole interactions, and correlated hopping processes. This applies to the chain [21], to the square lattice [41,42], and generally to the three-dimensional case [4] at half-filling, but also in the vicinity of half-filling, i.e., for finite doping [43].

We proceed in two steps. First, we consider very large U , i.e., we omit all terms of order t_0^2/U and only keep terms of order U and t_0 . This is the case studied in the literature. To our knowledge, almost all studies exclude the spin dynamics, i.e., flips of adjacent spins, except for brute force numerical studies and a preliminary statement on moments of the spectral density by Brinkman and Rice [4]. Second, we include the terms of order t_0^2/U to study to which extent they induce changes in the spectral densities including the character of the band edges. Such changes are expected, for instance the critical U deviates from W in the estimate $U_c \approx 1.10W$ obtained by Reischl *et al.* [42] for the square lattice. It turns out that band tails beyond the bare bandwidth are an important aspect that we will link to spin dynamics.

A semianalytic and a numerical approach are employed. The first, semianalytic approach relies on iterated equations of motion (iEoM) in the Heisenberg picture. The set of tracked operators is enlarged iteratively by commuting with the Hamiltonian, i.e., by applying the Liouville superoperator. This Liouvillian acts on operators like a Hamiltonian acts on states [44,45] yielding a Hermitian, oscillatory dynamics. The dominant part of the Liouvillian is the commutation with the hopping projected in such a way that no double occupancies are created or annihilated. Thus, the semianalytic approach amounts to a systematic expansion in the hopping element, which means in $x := t_0/U$. The second, numerical approach tracks the hole motion in time on finite clusters with periodic boundary conditions in 1D and 2D by the Chebyshev polynomial expansion technique (CET) [46–48]. We opt for the CET in place of exact diagonalization because the latter would require us to diagonalize the full Hamiltonian so that only

smaller systems can be treated, while the CET only requires that a few vectors of the finite-dimensional Hilbert space can be stored.

This article is structured in the following way: In Sec. II, the Hubbard model and its simplification in the limit of strong interaction is explained briefly. Section III outlines the concepts and algorithms used to assess the time evolution of observables and to gain insight into the metal-insulator phase. Section IV provides data in the time domain comparing results from the two approaches used, and it illustrates how band edges are determined. In Secs. V and VI we discuss the results for the generalized t - J model in 1D and 2D, respectively. A summary and outlook are given in Sec. VII.

II. INITIAL MODEL

The Fermi-Hubbard model is one of the prime examples and archetypical models for strongly interacting electrons on lattices, and it combines tight-binding electrons with a strongly screened, local Coulomb interaction [49–51]. We restrict our considerations to the one-band model in the vicinity of half-filling such that the Hamiltonian takes the form

$$H = H_0 + H_{\text{int}}, \quad (1a)$$

$$H_0 = t_0 \sum_{\langle i,j \rangle, \sigma} (f_{i\sigma}^\dagger f_{j\sigma} + \text{H.c.}), \quad (1b)$$

$$H_{\text{int}} = U \sum_i \left(\hat{n}_{i\uparrow} - \frac{1}{2} \right) \left(\hat{n}_{i\downarrow} - \frac{1}{2} \right). \quad (1c)$$

Here, $f_{i\sigma}^\dagger$ ($f_{i\sigma}$) are the creation (annihilation) operators at site i for a fermion of spin σ , $\hat{n}_{i\sigma}$ is the corresponding number operator, t_0 denotes the real hopping matrix element between the sites i and j , and $U > 0$ is the on-site interaction. The energy $U/2$ represents the energy cost of adding an electron inducing a double occupancy (DO) of two electrons at one site or of adding a hole inducing a double occupancy of holes at one site, i.e., creating an empty site. The kinetic energy H_0 is diagonal in momentum space with the dispersion relation

$$\varepsilon_{\mathbf{k}} := 2t_0 \sum_{i=1}^d \cos(\mathbf{k}\mathbf{a}_i) \quad (2)$$

with \mathbf{a}_i denoting primitive translation vectors spanning the underlying Bravais lattice. The model is particle-hole symmetric on bipartite lattices such as the 1D chain or the 2D square lattice.

A. Charge gap

A large enough on-site interaction $U > 0$ splits the local density of states $\rho(E)$ into a lower Hubbard band (LHB) and an upper Hubbard band (UHB) as shown in Fig. 1. This is the characterizing feature of a Mott insulator.

For general lattices, it is not known at which critical interaction strength U_c the gap finally closes signaling the instability of the Mott insulator. The 1D chain is special due to its integrability. It is solved exactly by thermodynamic Bethe ansatz equations [33] at any temperature. But also under the assumption of a disordered spin background and charge excitations at zero temperature, the problem can

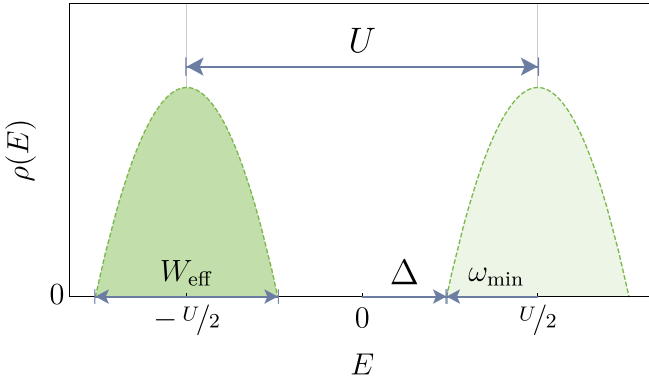


FIG. 1. For a large enough $U > 0$, the local density of states $\rho(E)$ splits into a lower and an upper Hubbard band at half-filling. Each band has the effective bandwidth W_{eff} . Charge excitations take the form of DOs of electron or hole character with a minimum excitation energy of the gap Δ . Decreasing the on-site interaction reduces the gap until it closes at the critical interaction U_c .

be treated analytically [34]. Yet we are not aware that the spectral density of the Hubbard models has been determined exactly by the Bethe ansatz. Another possibility at finite temperatures in 1D is to use time-dependent density matrix renormalization-group computations to determine spectral properties as well [14]. The complementary limit of a Bethe lattice with an infinitely large coordination number $z \rightarrow \infty$ can be treated by dynamic mean-field theory providing information on the local spectral densities [23–30]. But it must be stressed that in this limit, no spin dynamics takes place [9,11].

B. Effective model: Generalized t - J model

In the limit of strong interaction, i.e., $x = t_0/U \ll 1$, the Hubbard model can be mapped to t - J models based on perturbation theory in the small parameter x . First, we consider all terms linear in U , i.e., in zeroth order, as well as the hopping H_0 , which is of first order $xU = t_0$,

$$H_{\text{eff}} = H_{\text{int}} + T_0 + O(x^2U), \quad (3)$$

where T_0 stands for hopping processes without changes of the number of DOs; for its concrete definition, see below. In a further step, we include terms of second order $O(x^2U)$ step by step neglecting cubic and higher orders. The systematic derivation of the corresponding effective Hamiltonian can be done perturbatively [21,22,35–39,41] or via continuous unitary transformations [40,42,43,52–54]. Below, we quote the explicit results needed for the present work.

For the sake of brevity, we will use the term (generalized) t - J model even if the magnetic exchange is not present. Its effective hopping processes can be split in the following way:

$$H_{0,\text{eff}} = T_0 + T'_0 + T'_{s,0} + T''_0 + T''_{s,0}. \quad (4)$$

The magnetic exchange interaction can easily be added to $H_{0,\text{eff}}$; see below.

In (4), the term T_0 describes NN hopping from site i to j and *vice versa* subjected to the restraint that DOs are neither

added nor removed,

$$T_0 = t_0 \sum_{\langle i,j \rangle, \sigma} [(1 - n_{i,\sigma}) c_{i,\bar{\sigma}}^\dagger c_{j,\bar{\sigma}} (1 - n_{j,\sigma}) + n_{i,\sigma} c_{i,\bar{\sigma}}^\dagger c_{j,\bar{\sigma}} n_{j,\sigma} + \text{H.c.}]. \quad (5)$$

Here and in the following, the sums imply a one-time counting of each bond between the lattice sites i and j , and $\bar{\sigma}$ denotes the opposite of the spin orientation σ . We stress that this model is not fully equal to what is commonly referred to as the t - J model in the literature and textbooks since no magnetic interaction is taken into account. Nevertheless, this case is what is considered mostly in the context of single hole hopping in various spin backgrounds.

Hopping processes between next-nearest neighbors (NNN), i.e., all processes between sites on the 2D square lattice that lie on adjacent *diagonal* positions, are denoted by

$$T'_0 = t'_0 \sum_{\langle\langle i,j \rangle\rangle, \sigma} [(1 - n_{i,\sigma}) c_{i,\bar{\sigma}}^\dagger c_{j,\bar{\sigma}} (1 - n_{j,\sigma}) - n_{i,\sigma} c_{i,\bar{\sigma}}^\dagger c_{j,\bar{\sigma}} n_{j,\sigma} + \text{H.c.}]. \quad (6)$$

Hopping processes between third-nearest-neighbor (3NN) sites, i.e., sites that lie in-line on one of the axes and are separated by two bonds, are captured by

$$T''_0 = t''_0 \sum_{\langle\langle\langle i,j \rangle\rangle\rangle, \sigma} [(1 - n_{i,\sigma}) c_{i,\bar{\sigma}}^\dagger c_{j,\bar{\sigma}} (1 - n_{j,\sigma}) - n_{i,\sigma} c_{i,\bar{\sigma}}^\dagger c_{j,\bar{\sigma}} n_{j,\sigma} + \text{H.c.}]. \quad (7)$$

In 1D, only the second type, i.e., the contribution T''_0 , exists because there are no diagonals so that the double-prime processes represent NNN hopping. Since this makes the nomenclature NN, NNN, and 3NN ambiguous if 1D and 2D are both considered, we use the terms *prime* and *double-prime* hopping instead. In 2D, both exist; in 1D, only the double-prime hopping exists.

Apart from the above hopping processes, further *spin-dependent* hops occur in the effective model. Whenever charges hop from one site to another, e.g., from i to j , with a NN site k in-between, spin-dependent hops of the form

$$T'_{s,0} = t'_s \sum_{\substack{\langle\langle i,k,j \rangle\rangle \\ \alpha,\beta}} \{ [(1 - n_{i,\alpha}) c_{i,\bar{\alpha}}^\dagger \sigma_{\bar{\alpha},\bar{\beta}} c_{j,\bar{\beta}} (1 - n_{j,\beta})] \cdot \mathbf{S}_k + [n_{i,\alpha} c_{i,\bar{\alpha}}^\dagger \sigma_{\bar{\alpha},\bar{\beta}} c_{j,\bar{\beta}} n_{j,\beta}] \cdot \mathbf{S}_k + \text{H.c.} \}, \quad (8a)$$

$$T''_{s,0} = t''_s \sum_{\substack{\langle\langle\langle i,k,j \rangle\rangle\rangle \\ \alpha,\beta}} \{ [(1 - n_{i,\alpha}) c_{i,\bar{\alpha}}^\dagger \sigma_{\bar{\alpha},\bar{\beta}} c_{j,\bar{\beta}} (1 - n_{j,\beta})] \cdot \mathbf{S}_k + [n_{i,\alpha} c_{i,\bar{\alpha}}^\dagger \sigma_{\bar{\alpha},\bar{\beta}} c_{j,\bar{\beta}} n_{j,\beta}] \cdot \mathbf{S}_k + \text{H.c.} \} \quad (8b)$$

occur. These processes involve the hopping of a fermion over a nearest neighbor and its interaction with the spin of this nearest neighbor. For instance, the spin of the hopping fermion can swap with the spin of the nearest neighbor. Just like the hopping processes in (6) and (7), the spin-dependent processes (8) do not change the overall number of DOs. As before, in 1D only the double-prime processes exist because of the lack of diagonals. The leading second order of these processes

is determined analytically via perturbation theory [4,21,41] or numerically by CUTs [42]. In the following we use the analytical values, which read in 1D [21]

$$t'' = -\frac{t_0^2}{2U}, \quad (9a)$$

$$t_s'' = \frac{t_0^2}{U}. \quad (9b)$$

Generalizing to 2D, there is exactly one shortest route from i to j which generates the t'' contribution. For diagonal hopping, i.e., for t' , there are two shortest routes. A diagonal hop on a square lattice can happen via first a horizontal step and then a vertical step or *vice versa*. For spin-independent diagonal hopping, both routes contribute and hence one has a factor 2,

$$t' = -\frac{t_0^2}{U}. \quad (10)$$

For spin-dependent processes, the involved intermediate lattice site k distinguishes the two routes so that

$$t_s' = \frac{t_0^2}{U}; \quad (11)$$

no doubling occurs. These generalized prefactors (10) and (11) are consistent with the numerically determined prefactors t' and t_s' [42], and they agree with the 2D results in Ref. [41].

Next, we consider the spin-spin Heisenberg interactions appearing as well in second order. The model with NN hopping only and the spin-spin interactions is conventionally called the t - J model in the literature. The Heisenberg term reads

$$H_J = J \sum_{(i,j)} \mathbf{S}_i \mathbf{S}_j = \frac{J}{2} \sum_{(i,j)} \left(P_{ij} - \frac{1}{2} \right) \quad (12)$$

with $J = \frac{4t_0^2}{U}$ so that the total effective Hamiltonian of the generalized t - J model becomes

$$H_{\text{eff}} = H_{0,\text{eff}} + H_J. \quad (13)$$

The equivalent notation employing the permutation operator P_{ij} interchanging two spins $S = 1/2$ on the lattice sites i and j is useful in numerics where the spin states are represented by bit patterns.

In the sequel, we will use two choices for the magnetic exchange:

$$(A) \quad J = \frac{t_0}{3}, \quad (14a)$$

$$(B) \quad J = \frac{t_0}{d}. \quad (14b)$$

Choice (A) is a generic value relevant in many cuprates. Choice (B) represents the maximum value of the magnetic exchange because for larger hopping the mapping of the Fermi-Hubbard model to a (generalized) t - J model no longer makes sense because the Mott insulator description breaks down if the bandwidth $W = 4dt_0$ reaches U .

III. METHODS

Here, we briefly introduce the methods used in the present study to keep it self-contained. Strengths and shortcomings of the techniques are pointed out, and uncommon technical aspects are discussed. The iEoM approach works in the Heisenberg picture addressing operators while the Chebyshev expansion treats quantum states. The iEoM approach systematically truncates the underlying Hilbert space of operator monomials, but it treats the thermodynamic limit of an infinite lattice. The CET considers the whole Hilbert space with exponentially increasing dimension for increasing finite system size. For the iEoM approach, no simulation of the time dependence of the hole-doped generalized t - J model up to a specific threshold time t_{max} is necessary. Instead, the excitation spectrum can be deduced by diagonalization.

A. Iterated equations of motion

We follow here the previous applications in Refs. [55–57] using a suitable scalar product [44,45]. But other variants of iterated equations of motion have been used in abundance in the literature. The basic idea is to expand a time-dependent arbitrary operator $A(t)$ in the Heisenberg picture in a basis of time-independent operators $\{A_i\}$

$$A(t) = \sum_i h_i(t) A_i. \quad (15)$$

All time dependence is contained in the complex prefactors $h_i(t)$. The Heisenberg equation of motion reads

$$\frac{d}{dt} A(t) = i[H(t), A(t)] =: i\mathcal{L}(A(t)) \quad (16)$$

with the Liouville superoperator $\mathcal{L}(\cdot)$ leading to

$$\frac{d}{dt} A(t) = i \sum_i h_i(t) \mathcal{L}(A_i). \quad (17)$$

Expanding $\mathcal{L}(A_i)$ in the chosen basis $\{A_i\}$ is achieved by

$$\mathcal{L}(A_i) := \sum_j M_{ji} A_j \quad (18)$$

defining the Liouvillian matrix \mathbf{M} , also called the dynamic matrix. This enables the compact notation

$$\frac{d}{dt} \mathbf{h}(t) = i\mathbf{M}\mathbf{h}(t). \quad (19)$$

If the basis $\{A_i\}$ is orthonormal, the matrix elements of \mathbf{M} are given directly by

$$M_{ji} = (A_j | \mathcal{L}(A_i)). \quad (20)$$

If the Liouvillian is self-adjoint with respect to the chosen scalar product, \mathbf{M} is Hermitian. This is the case for the Frobenius scalar product

$$(A|B) := \mathcal{N} \text{Tr}(A^\dagger B) \quad \text{with} \quad \mathcal{N} := 1/\text{Tr}(\mathbb{1}) \quad (21)$$

if the local Hilbert space of a single site is finite-dimensional [44,45].

To describe the hopping of a single hole, we start from the insertion of a single hole at site i by the operator $K_i = \bar{h}_{i\uparrow} = f_{i\downarrow} f_{i\uparrow} f_{i\uparrow}^\dagger$. Further operators A_j are created by iterated application of $\mathcal{L}(\cdot)$. Since we restrict ourselves to one

hole away from strict half-filling, it is sufficient to consider a product of spin operator at sites j with $B_j = \sigma_j^+ = f_{j\uparrow}^\dagger f_{j\downarrow}$, $B_j = \sigma_j^- = f_{j\downarrow}^\dagger f_{j\uparrow}$, or $B_j = \sigma_j^z = f_{j\uparrow}^\dagger f_{j\uparrow} - f_{j\downarrow}^\dagger f_{j\downarrow}$. Then the operator basis consists of monomials of the form

$$A_m = N_m K_i(C_m) \prod_{j \in C_m} B_j(C_m), \quad (22)$$

where the argument C_m defines the set of sites (cluster) involved and which operator of the choices given above is to be taken. The normalization factor is given by N_m .

Once the operator basis of monomials A_m is determined, the dynamic matrix \mathbf{M} is calculated using (20) and diagonalized leading to the desired set of eigenvalues ω_n and the corresponding eigenvectors \mathbf{v}_n . For efficiency, we resort to the Lanczos algorithm [58] because the Hermiticity of \mathbf{M} is guaranteed by construction. The Lanczos algorithm generates an f -dimensional Krylov space; the eigenvalues and eigenvectors in the Krylov space are denoted $\bar{\omega}_n$ and $\bar{\mathbf{v}}_n$, respectively. To very good accuracy, the dynamics of an operator can be found as the linear combination

$$\mathbf{h}(t) = \sum_{n=1}^f \alpha_n e^{i\bar{\omega}_n t} \bar{\mathbf{v}}_n \quad (23)$$

with the coefficients α_n chosen such that the initial condition is fulfilled. We varied the dimension f of the Krylov space to monitor if any changes in the results occur, and finally we chose $f = 200$, above which no changes are discerned anymore. In particular, the minimum of $\bar{\omega}_n$ represents a very reliable estimate for the band edge. As long as $U/2 + \bar{\omega}_n > 0$, the Mott insulating phase is locally stable.

Since we consider a fully disordered spin background, the initial hole is not inserted in a pure state, but in a mixture captured by the density matrix

$$\rho_0 \propto \mathbb{1} \quad (24)$$

in spin space. The subsequent dynamics is described by the retarded Green's function,

$$g(t) = -i \text{Tr} (\bar{h}_{i\uparrow}(t) \bar{h}_{i\uparrow}^\dagger \rho_0) \theta(t), \quad (25)$$

where $\theta(t)$ is the Heaviside function. No commutator appears because its second term vanishes because no hole can be annihilated in the exactly half-filled state. Eventually, one obtains

$$g(t) = -i \langle \bar{h}_{i\uparrow}(t) \bar{h}_{i\uparrow}^\dagger(0) \rangle \theta(t) \quad (26a)$$

$$= -i \sum_{mn} \bar{h}_m(t) h_n^*(0) \langle A_m A_n^\dagger \rangle \theta(t) \quad (26b)$$

$$= -i \sum_n |\alpha_n|^2 e^{i\bar{\omega}_n t} \theta(t), \quad (26c)$$

where orthonormality is used. The spectral density $A(\omega)$ results from the Fourier transform $g(\omega)$ of (26c),

$$A(\omega) = -\frac{1}{\pi} \text{Im} g(\omega) \quad (27a)$$

$$= \sum_n |\alpha_n|^2 \delta(\omega - \bar{\omega}_n), \quad (27b)$$

wherein the squared modulus of α_n indicates the weight and hence the relative importance of the corresponding process for the hole dynamics.

A finite number of applications of $\mathcal{L}(\cdot)$, i.e., a finite order m , implies that only processes with a finite spatial spread in the infinite system are taken into account. Hence only a finite number of eigenvalues ω_n occurs so that the spectral density (27a) is not continuous, but consists of discrete δ -peaks even if the Krylov dimension f would be chosen maximal. We checked that doubling f does not influence the obtained numerical results. The loop order m cannot be increased easily. To compare continuous spectral densities from different approaches, we broaden the δ -peaks by Gaussians,

$$A(\omega) = \sum_n \frac{|\alpha_n|^2}{\sqrt{2\pi}\sigma} \exp\left(-\frac{(\omega - \bar{\omega}_n)^2}{2\sigma^2}\right). \quad (28)$$

This broadening σ has the unit of an energy; recall that we set $\hbar = 1$. The chosen values of σ will be discussed below.

B. Chebyshev expansion technique

The Chebyshev expansion technique is a very well established technique to evolve quantum states in finite Hilbert spaces in time [46,47]. The basic idea is to expand the time evolution operator in terms of Chebyshev polynomials T_n ,

$$\exp(-iHt) = \sum_{n=0}^{\infty} \alpha_n(t) T_n(H'), \quad (29a)$$

$$\alpha_n(t) = (2 - \delta_{n,0}) i^n e^{-ibt} J_n(at), \quad (29b)$$

where H' is the rescaled Hamiltonian $H \rightarrow H' = (H - b)/a$ so that the spectrum of H' lies in the interval $[-1, 1]$. The time dependence is essentially given by the Bessel functions J_n . The error ϵ due to truncation of the infinite series at order N_c in the above equation can be systematically controlled according to

$$\epsilon \lesssim \left(\frac{at_{\max} e}{2N_c}\right)^{N_c}, \quad (30)$$

where t_{\max} is the maximum time considered.

The spectral density is computed via the retarded Green's function $g(t)$. The trace over the half-filled Hilbert space in (25) is determined by stochastic trace evaluation as proposed by Skilling [59] and generalized later [47,60,61]. The full trace $\text{Tr}(A)$ by $R \ll d$ is approximated by the sum over R normalized states $|r\rangle$ whose complex coefficients are each drawn from a normal distribution

$$\text{Tr}(O) = d \langle \overline{|r\rangle \langle O | r} \rangle, \quad (31)$$

where the overbar denotes the arithmetic average over the R random states, and d is the dimension of the half-filled Hilbert space on the finite cluster considered. The standard deviation of the estimate (31) scales like $1/\sqrt{Rd}$. Finally, inserting (31) and (24) into (25) yields the Green's function

$$g(t) \approx -\frac{i}{R} \sum_{r=1}^R \langle r | e^{iH_{\text{eff}} t} \bar{h}_{i\uparrow} e^{-iH_{\text{eff}} t} \bar{h}_{i\uparrow}^\dagger | r \rangle \theta(t). \quad (32)$$

We consider the hole dynamics in both the generalized t - J model in its form H_{eff} as well as the hopping-only model

$H_{0,\text{eff}}$. In the latter case, one can simplify the above expression to

$$g_{0,\text{eff}}(t) \approx -\frac{i}{R} \sum_{r=1}^R \langle r | \bar{h}_{i\uparrow} e^{-iH_{0,\text{eff}}t} \bar{h}_{i\uparrow}^\dagger | r \rangle \theta(t), \quad (33)$$

because $e^{iH_{\text{eff}}t}$ has no effect for $J = 0$ on $|r\rangle$ because no hopping can take place at $\langle r|$.

The Green's functions (32) and (33) are calculated for a finite time span $[0; t_{\text{max}}]$ and then Fourier-transformed,

$$g(\omega) := \sum_n e^{-i\omega t_n} g(t_n) dt. \quad (34)$$

The finite time interval leads to spurious ringing in the Fourier transforms (34), which we suppress by multiplying the temporal Green's function $g(t)$ with a gradually decreasing function. For simplicity, we opt for Gaussian damping

$$\tilde{g}(t) = g(t) \exp(-t^2/(2\sigma^2)), \quad (35)$$

which amount to the convolution with the Gaussian kernel $K \propto \exp(-\omega^2/2\sigma^2)$ in the frequency domain. Finally, the spectral density reads

$$A(\omega) = -\frac{1}{\pi} \text{Im} \tilde{g}(\omega). \quad (36)$$

IV. REAL TIME DEPENDENCE AND BAND EDGES

A. Method comparison

Here we compare the two methods described in Sec. III for the complete generalized t - J model in (13) on the 1D chain with the parameters (A) in (14a). In all of the following results, the hopping element t_0 defines the energy unit and the time unit $[t] = 1/t_0$.

Using (26) and (32), the retarded Green's function $g(t)$ is displayed in Fig. 2. The short-time behavior of $g(t)$ is determined analytically by expanding in powers of t (cf. Appendix A); see the dashed blue line. The Green's function starts at $g(t=0) = 0.5$ because a hole can only be created if an electron with the appropriate spin is present. Due to the assumed spin disorder, this holds in 50% of the cases.

The time dependence in Fig. 2 resembles a damped oscillation. But in a closed quantum system, no relaxation can occur so that the damping must be seen as dephasing from the superposition of many coherent oscillations. Since we are dealing with a large mixture of spin backgrounds, it is plausible that this strong dephasing results from very many eigenstates of the hole motion. In CET, no finite-size effects appear in the studied time interval up to $t_{\text{max}} = 20$ (not fully shown here) as supported by the agreement of the results for $N = 10, 14$, and 18 . For this reason, we refrain from further analysis of finite-size effects in subsequent CET results. The iEoM results agree very well with the CET data except for low loop order m . We emphasize that the iEoM dynamics consists of oscillatory contributions exclusively; no contributions to $g(t)$ decrease or increase exponentially due to the guaranteed Hermiticity of the dynamic matrix [44,45].

For the iEoM data, we use the maximum available loop order m . It strongly depends on the lattice as well as on

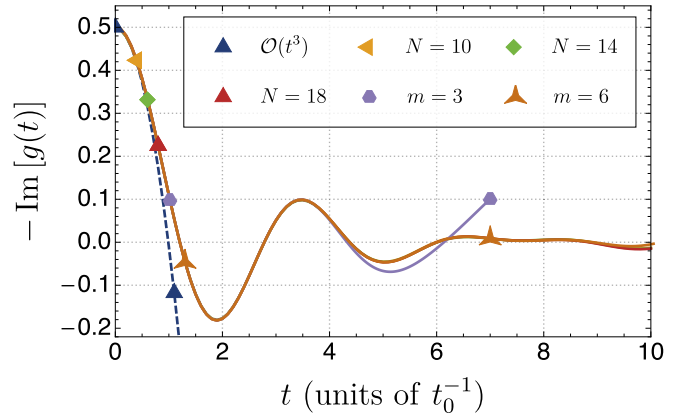


FIG. 2. Retarded Green's function of the chain for the complete generalized t - J model with parameters (A) for various chain lengths N (CET) and loop orders m (iEoM). The parabola (blue triangles) from the expansion, cf. Appendix A, in powers of t up to $O(t^3)$ is depicted for orientation. The iEoM result for $m = 6$ first starts to deviate from the CET results at about $t \geq 9/t_0$.

the number of physical processes considered. The number of processes depends on whether only first-order contributions in t_0/v with T_0 , second-order contributions without spin-spin interaction ($H_{0,\text{eff}}$), or the complete generalized t - J model is considered. The numerically most challenging case is given by a high coordination number z and the complete generalized t - J model, i.e., for 2D and H_{eff} . For this case, we reached $m = 3$ at most due to memory constraints.

B. Determination of band edges

A particularly interesting issue is the width of the Hubbard bands. Note that this implies the existence of finite band edges. Otherwise, the width would be infinite. So far, the literature considered band tails, but with finite band edges not exceeding the bare edges [4,9,11]. We are interested in the lower band edge of the upper Hubbard band. In the particle-hole symmetric case, this is equivalent to the upper band edge of the lower Hubbard band, which describes the hole motion. The necessary minimum energy eigenvalue ω_{min} can be determined systematically from the iEoM results by extrapolating $\omega_{\text{min}}(m)$ in the loop order $m \rightarrow \infty$. This procedure considers the infinite system and takes processes of larger and larger spatial range into account upon increasing m . If $m \rightarrow \infty$ were realizable, the result would be exact.

Data are shown in Fig. 3 for the chain and parameters (A), cf. (14a); the results for parameters (B), cf. (14b), are qualitatively the same. The more processes included in the Hamiltonian, the lower is the maximum loop order m achieved. If the minimum eigenvalues converge toward a finite value

$$c := -\omega_{\text{min}}(m \rightarrow \infty), \quad (37)$$

this value yields the exact band edge. To estimate this value, we fit the data by

$$-\omega_{\text{min}}(m) = \frac{a}{(m-b)} + c. \quad (38)$$

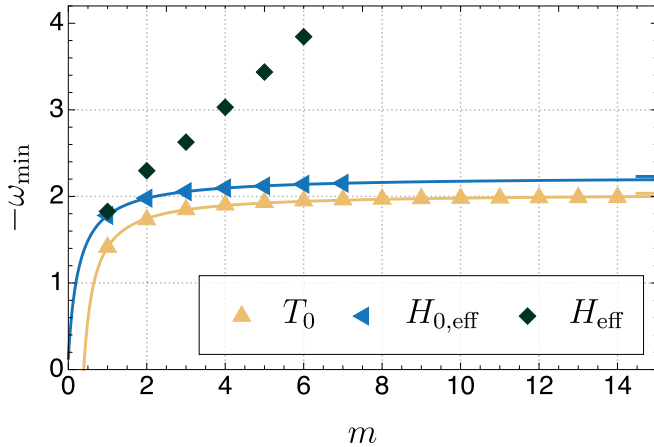


FIG. 3. Minimum eigenvalues ω_{\min} (symbols) for a chain and parameters (A) as a function of the loop order m of the iEoM. The three different Hamiltonians [NN hopping only (T_0), generalized hopping in second order ($H_{0,\text{eff}}$), and the inclusion of magnetic exchange (H_{eff})] are shown by different colors. The solid lines mark fits of the form (38) where applicable. The fit parameter $c = -\omega_{\min}(m \rightarrow \infty)$ is displayed as short horizontal bars at the right boundary of the graph.

These fits are displayed by solid lines in Fig. 3; they describe the depicted data very well for the effective models comprising only hopping, i.e., for the Hamiltonians T_0 and $H_{0,\text{eff}}$. The key observation, however, is that the data for the Hamiltonian including the magnetic exchange look qualitatively very different. Instead of a hyperbolic behavior, the data appear to diverge linearly with m . Although it might be that the data converge to some finite value, at much higher values of m the qualitative difference from the hopping-only cases catches the eye. If the data diverge, this indicates an *unbounded* support of the corresponding Hubbard band.

Clearly, the qualitative difference is related to the magnetic exchange and hence to the spin dynamics, which has been hitherto mostly neglected. We consider the magnetic energies in order to reach a physical understanding of the observation. In the antiferromagnetic Heisenberg model without a hole, the eigenenergies lie in the interval between the ground-state energy $E_{\min} < 0$ and the maximum energy for fully polarized states $E_{\max} > 0$. Both limits are extensive, i.e., they are proportional to the system size N and hence for the infinite system infinitely negative and positive, respectively. In contrast, the energy expectation value of any of the completely disordered initial spin states is zero. Hence, according to the Lehmann representation of spectral densities, contributions to the spectral density can stem from transitions between the initial disordered spin states and the eigenstates at energies between $-\infty$ and ∞ if the corresponding matrix elements do not vanish. For this reason, an unbounded support is possible. It is not ruled out by energy reasons. At this stage, we cannot prove that the matrix elements are finite. But there is no reason why the matrix elements should vanish for the infinite number of eigenstates with extensively negative or positive eigenenergies. Further analysis of our data addressing the shape of the spectral tails will be provided below.

Our observation and argument pointing toward an infinite support of the density of states (DOS) seems to contradict the findings of Ejima and co-workers [34], who studied the 1D Hubbard model by the Bethe ansatz under the assumption of a completely disordered spin background. They identified and computed a finite lower band edge for the charge excitations. Since the generalized t - J model can be derived from the Hubbard model in the Mott insulating phase for large interaction U , one does not expect a qualitative difference in the support of the spectral density. But in the treatment of the charge dynamics by the Bethe ansatz, the dynamics of the spin sector has been treated as frozen [34]. This means that the balance of magnetic energies has not been included because the focus was on the influence of the disordered spin states on the charge excitations, but not on the spin *dynamics*. Hence, the considered quantities differ and the contradiction is only apparent.

V. RESULTS FOR THE CHAIN

We consider explicit results for the local spectral densities and their lower band edges where detectable. First, however, we study the tails of the spectral densities where no band edges are found.

A. Tails of the spectral densities

Above, we found indications that the spectral density differs qualitatively depending on whether the magnetic exchange is considered. One indication was numerical, while the other was the analytic argument that the energy balance of the spin degrees of freedom allows for contributions at all frequencies from $-\infty$ to ∞ if the matrix elements do not vanish for large parts of Hilbert space. In this section, we address what the numerical results tell us about the matrix elements and the resulting tails of the spectral densities.

The starting point is the fact that the orientation of each spin at half-filling is chosen randomly and independently for each site in the completely disordered spin ensemble. Hence, an infinite number of independent random processes influences the matrix elements entering the spectral densities and their tails in particular. The central limit theorem suggests that the resulting tails are of Gaussians nature. This working hypothesis is consistent with the indications for an infinite support of the spectral densities. Next, we put the working hypothesis to a quantitative numerical test.

For this test we have to refrain from any broadening because this would induce artificial tails concealing the intrinsic physics. Similar to mathematical studies on probability distributions, we focus on the primitive of the spectral densities because it is unambiguously defined even for discrete distributions. We define

$$f_-(\omega) = \int_{-\infty}^{\omega} A(x) dx, \quad (39a)$$

$$f_+(\omega) = \int_{\omega}^{\infty} A(x) dx, \quad (39b)$$

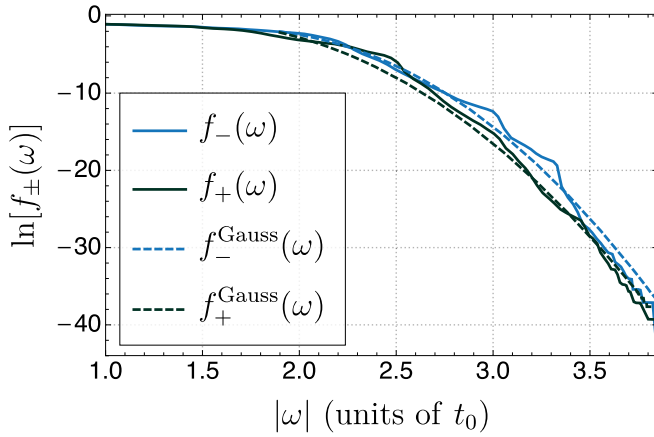


FIG. 4. Analysis of the lower and the upper tail of the spectral density as obtained by iEoM via the logarithm of the primitives defined in Eq. (39) for the parameter set (A); the fits are defined in Eq. (40). The optimum fit parameters read $W_- = 0.28$, $\sigma_- = 0.24t_0$, $x_- = -1.88t_0$ for the lower tail, and $W_+ = 0.80$, $\sigma_+ = 0.26t_0$, $x_+ = 1.62t_0$ for the upper tail.

where f_- is used to study the lower tail $\omega \rightarrow -\infty$ and f_+ is used for the upper tail $\omega \rightarrow \infty$. If the tails were close to Gaussian, the following approximate relations would hold:

$$f_-(\omega) \approx f_-^{\text{Gauss}}(\omega) \quad (40a)$$

$$:= \frac{W_-}{\sqrt{2\pi}\sigma_-} \int_{-\infty}^{\omega} \exp\left(-\frac{(x-x_-)^2}{2\sigma_-^2}\right) dx \quad (40b)$$

$$= \frac{W_-}{2} [\text{erf}(\omega_-) + 1], \quad (40c)$$

$$f_+(\omega) \approx f_+^{\text{Gauss}}(\omega) \quad (40d)$$

$$:= \frac{W_+}{\sqrt{2\pi}\sigma_+} \int_{\omega}^{\infty} \exp\left(-\frac{(x-x_+)^2}{2\sigma_+^2}\right) dx \quad (40e)$$

$$= \frac{W_+}{2} [1 - \text{erf}(\omega_+)], \quad (40f)$$

where

$$\omega_- := (\omega - x_-)/(\sqrt{2}\sigma_-), \quad (41a)$$

$$\omega_+ := (\omega - x_+)/(\sqrt{2}\sigma_+). \quad (41b)$$

Three free parameters need to be determined by fitting. Since exponentially small values of the f -functions occur, we plot $\ln(f_{\pm})$ as a function of $|\omega|$ in Fig. 4 and compare it with the fits (40). The fitted parameters are given in the caption. The corresponding results for the parameter set (B) can be found in Fig. 5.

The agreement between the data obtained by iEoM and the fits is very good. The logarithm of the iEoM data clearly shows an approximate parabolic shape consistent with Gaussian tails even though some fluctuations occur. For comparison, we note that an exponential tail would yield straight lines in the logarithmic plots. But we point out that the agreement found for all four fits extends over 15 orders of magnitude if one converts the differences on the log-scale to decimal ratios. We take this observation as support for the hypothesis of Gaussian tails. To our knowledge, brute force

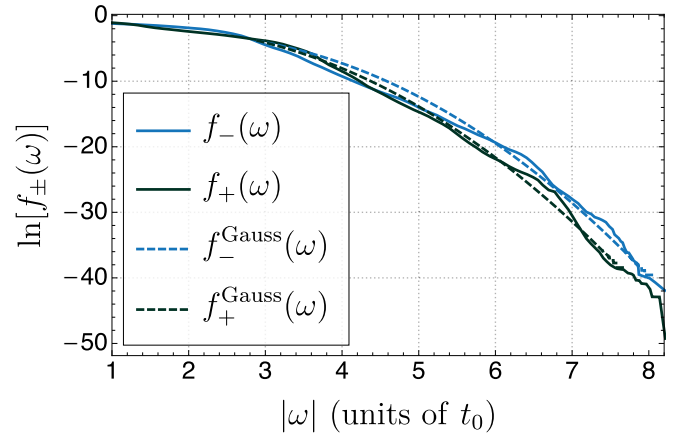


FIG. 5. Same as Fig. 4, but for parameters (B) and the fit parameters $W_- = 0.12$, $\sigma_- = 0.69t_0$, $x_- = -2.26t_0$ for the lower tail, and $W_+ = 0.37$, $\sigma_+ = 0.70t_0$, $x_+ = 1.81t_0$ for the upper tail.

numerical approaches can hardly provide information over such a range of energies.

The analogous analyses in 2D are currently not conclusive because of the low maximum loop order m . But the preliminary results point in the same direction as in 1D. In view of the conceptual relevance of this issue, further studies are called for.

B. Spectral densities

The spectral densities $A(\omega)$ for the chain for the three cases T_0 , $H_{0,\text{eff}}$, and H_{eff} are displayed in Figs. 6 and 7. For $H_{0,\text{eff}}$ and H_{eff} the difference of the two parameter sets (A) and (B) matters. The results from the different methods used, CET (solid) and iEoM (dashed), agree very well in all cases. The data have been broadened by $\sigma = 0.15t_0$ to reach continuous curves which are little influenced by finite size or finite loop effects. The first three moments of the spectral densities can be computed by CET and by iEoM and they agree, but they differ qualitatively from the results by Brinkman and Rice [4]; for instance, the first moment vanishes rigorously.

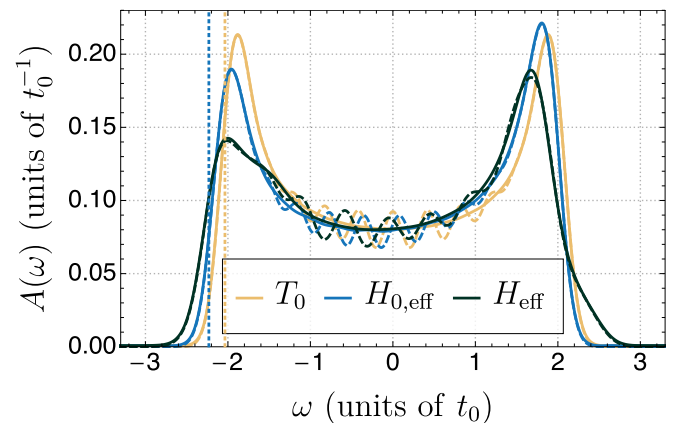


FIG. 6. Spectral density $A(\omega)$ vs ω for a chain and the parameter set (A) in (14a), broadened by $\sigma = 0.15t_0$. Solid lines represent CET results, dashed lines iEoM results. The band edges ω_{min} determined from (37) are indicated by vertical dashed lines.

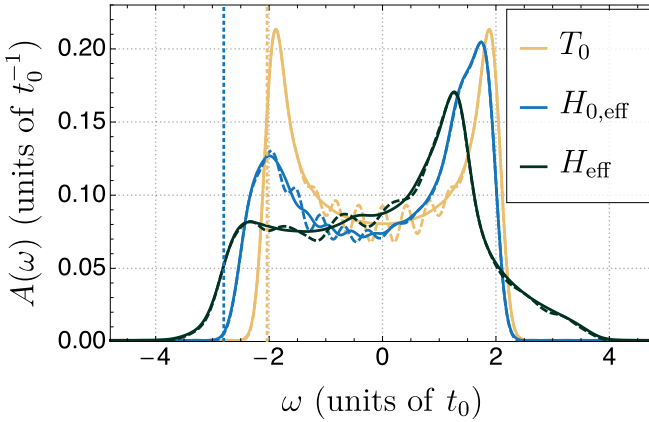


FIG. 7. Same as Fig. 6, but for the parameters (B) in (14b).

Both the upward and downward flanks of the spectral density as well as the characteristic shape including the peak positions are accurately reproduced. The wiggling of the iEoM results around $\omega = 0$ results from a few discrete, Gaussian broadened peaks. Higher loop order m and thus increased basis would lead to smoother spectral densities.

The spectral density $A(\omega)$ for T_0 is symmetric about $\omega = 0$. This is expected because T_0 represents NN hopping, which implies particle-hole symmetry on bipartite lattices and thus symmetric local DOS. This has been shown rigorously in the 1D case in the limit $U \rightarrow \infty$ [4,21,22]. The rigorous result also explains the value of the lower band edge $\omega_{\min} = -2t_0$, which our extrapolation reproduces well within a relative error of 2%. The pronounced peaks are the van Hove singularities $\propto 1/\sqrt{|\Delta\omega|}$, which are smeared out by finite-size effects or finite loop order and the additional broadening. The analytical results [4,21,22] yield the explicit result

$$A(\omega) = \frac{1}{2\pi} \frac{1}{\sqrt{\omega^2 - 4t_0^2}}. \quad (42)$$

If the spin-dependent and spin-independent hopping in second order is included, i.e., if we consider $H_{0,\text{eff}}$, the support of the spectrum increases: for parameter set (A) it increases by about 10%, and for set (B) it increases by almost 20%. Since the DOS satisfies the sum rule $\int A(\omega)d\omega = 1/2$, a larger support necessarily translates into a reduced average height. In addition, the DOS loses its symmetry: the left van Hove peak becomes lower than the right one.

If the magnetic exchange, i.e., the spin-spin interaction, is included, we consider the dynamics induced by H_{eff} . The corresponding data are shown by the darkest curves in Figs. 6 and 7. The broadened curves show a larger asymmetry between the left and the right peak compared to the curves for $H_{0,\text{eff}}$. For parameter set (B) the left peak is reduced to a shoulder only. The tails contain much more weight, in particular for parameter set (B). No band edge can be detected for the reasons discussed in the preceding section.

VI. RESULTS FOR THE SQUARE LATTICE

Analogous to calculations for the chain, spectral densities and band gaps can also be determined for the square lattice.

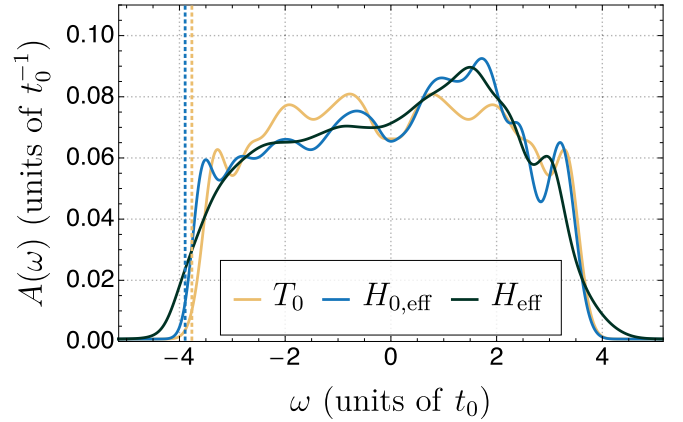


FIG. 8. Spectral density $A(\omega)$ for hole motion on the square lattice and parameter set (A). See the caption of Fig. 6 for further explanations.

We emphasize that such a calculation does not merely enlarge the dimension, but it introduces also additional physical processes along the diagonals. Furthermore, the four nearest neighbors in the square lattice, instead of two in the chain, yield a more densely populated Hamiltonian matrix. For the same tractable cluster size N , only \sqrt{N} hopping processes are possible without wraparound for NN hopping, and correspondingly fewer are possible for NNN or 3NN hopping. Thus, describing the dynamics without finite-size effects becomes significantly more demanding. As a result, the obtained densities are not as smooth as in 1D and they wiggle more. The iEoM treats the thermodynamic limit by construction, but it cannot reach the same accuracy as in 1D either because the additional physical processes reduce the maximum loop order m that can be reached. The first three moments of the spectral densities can be computed by CET and by iEoM and they agree, but they differ qualitatively from the results by Brinkman and Rice [4]; for instance, the first moment vanishes rigorously.

To realize more hopping processes without wraparound effects, we rotate the studied square cluster by 45° . Then its edge length is given by $\sqrt{2}n$, where n is the number of NN steps to pass from one corner of the square cluster to its center implying $N = 2n^2$. For $n = 3$ we have to treat 18 sites, which is still feasible while the wraparound only occurs after $2n = 6$ NN hops. Without the rotation this would have required $N = 6^2 = 36$ sites, and the corresponding Hilbert space dimension would have been larger by almost a factor 2.6×10^5 .

The overall shape of the spectrum is significantly altered compared to the 1D case; see Figs. 8 and 9 for CET results. Results obtained by iEoM are presented and compared to CET results for larger broadening in Appendix B. In contrast to the two distinct van Hove singularities in 1D, the 2D case reveals a spectral density of approximately elliptical or even rectangular shape. It is symmetric only for T_0 and becomes asymmetric as soon as the Hamiltonian is extended, in agreement with what was found in 1D. Note, however, that the lower band edge for T_0 is not $-4t_0$ but close to this value (see the vertical dashed lines in Figs. 8 and 9). This is in contrast to the 1D case, where we had found $-2t_0$. The reason is that in

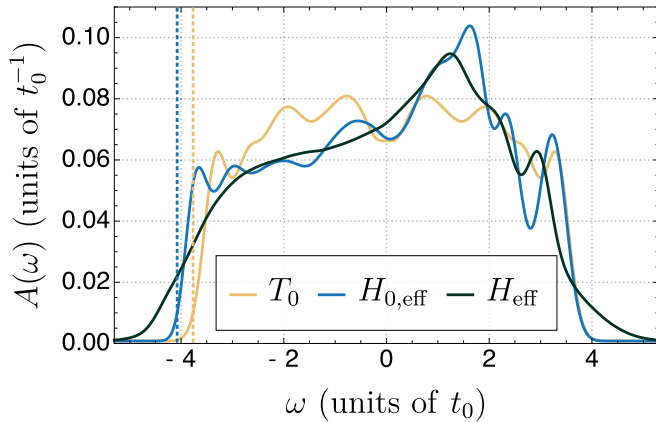


FIG. 9. Spectral density $A(\omega)$ for hole motion on the square lattice and parameter set (B). See the caption of Fig. 6 for further explanations.

1D at $U = \infty$, perfect spin-charge separation for NN hopping occurs, i.e., the sequence of spin orientations is not changed by the hole motion. On the square lattice, this is no longer true since loops occur allowing for subtle interferences. Only Trugman paths [5] allow for hole motion without changes of the spin order.

For the square lattice, the band edges ω_{\min} are significantly closer to each other than in 1D. For the parameter set (A) we attribute this to the altered dimensionality. For parameter set (B), this effect is enhanced by the smaller value of the exchange coupling J , i.e., because of $J_{1D,B} = 1 > 1/2 = J_{2D,B}$. We emphasize that our results agree with previous research, for instance $\omega_c = -4.4t_0$ for the complete generalized t - J model [42]. This value is in the range of the left flanks where the DOS starts rising significantly; cf. the black curves in Figs. 8 and 9. An exact determination of the band edge is not possible due to the previously discussed Gaussian tails.

Analogous to the 1D case, a broadening of the spectrum upon including more and more processes is observed also on the square lattice. For parameter set (A) the spectrum broadens from T_0 to the complete generalized t - J model H_{eff} by about 13 %; for parameter set (B) the spectrum broadens by almost 25 %. Instead of peaks at the boundaries of the DOS, one observes kneelike flanks. This can be attributed to the weaker van Hove singularities in 2D, which consist of either jumps or logarithmic divergences.

VII. SUMMARY AND OUTLOOK

We studied the dynamics of a single hole in a disordered spin background for various kinds of the generalized t - J model which result from the Fermi-Hubbard model in the limit of large repulsion U by eliminating systematically the processes changing the number of double occupancies. This can be done in or close to the Mott insulating phase. The systematic elimination is controlled by the small parameter $x = t_0/U$, where t_0 is the bare nearest-neighbor (NN) hopping. In second order in x , spin-dependent and spin-independent next-nearest-neighbor (NNN) hopping as well as the nearest-neighbor spin-spin exchange interaction appear yielding a generalized t - J model. (Often, the model consisting of the

projected NN hopping and the NN magnetic exchange is called the t - J model.) For the one-dimensional chain and the two-dimensional square lattice, we computed the lower band edges of the Hubbard bands where possible and the shape of the local spectral density, i.e., the density of states (DOS). This is achieved by two approaches, the iterated equations of motion (iEoM) and the Chebyshev expansion technique (CET).

The CET is a well-established numerically exact method for the analysis of finite clusters whose effort increases exponentially with the Hilbert space size. The iEoM addresses the infinite translationally invariant lattice, i.e., the thermodynamic limit. The systematic enlargement of the iEoM by increasing the loop order m includes processes of larger and larger spatial range. In 1D, numerical evidence was found and an analytic argument was given that the support of the DOS is only finite if hole hopping enters the Hamiltonian exclusively. Once magnetic exchange is switched on as well, the support becomes infinite and the DOS develops Gaussian tails. This effect has not yet been discussed in the literature to our knowledge because the spin dynamics is generically omitted. We point out that a previous analysis of the Hubbard model based on the Bethe ansatz found finite band edges for the hole motion in a disordered spin background [34]. But in this analysis, the spin dynamics was treated as frozen so that the magnetic energy balance did not enter. Hence, the results are not contradicting.

The analysis of the support of the spectral densities has become possible by means of the iEoM. Numerical evidence for Gaussian tails could be found in 1D, while the data in 2D are not yet conclusive. But the analytic argument in favor of an infinite support also holds in 2D. The substantially higher numerical effort in 2D calls for further efforts to corroborate the advocated scenario.

Future routes of research can address the spreading of a locally inserted hole in real space as it can be measured in ultracold atoms [16,17]. For solid-state systems, the momentum resolved spectral densities should be investigated.

ACKNOWLEDGMENTS

We gratefully acknowledge financial support by the Konrad Adenauer Foundation (P.B.) as well as by the German Research Foundation (DFG) in projects UH 90-13/1 (G.S.U.) and UH 90-14/1 (D.B.H.) and in project B8 of ICRC 160 (G.S.U.) together with the Russian Foundation for Basic Research. Parts of the calculations were performed on the LiDO3 high-performance computing system partially funded by the DFG. The authors are indebted to Fabian Essler, Florian Gebhard, Fabian Grusdt, and Matthias Vojta for helpful discussions.

P.B. and G.S.U. wrote the manuscript, D.B.H. computed the iEoM data and P.B. the CET data.

APPENDIX A: APPROXIMATION OF THE SHORT-TIME BEHAVIOR OF $g(t)$

The behavior of the retarded Green's function $g(t)$ for $t \gtrsim 0$ can be estimated analytically by an expansion in

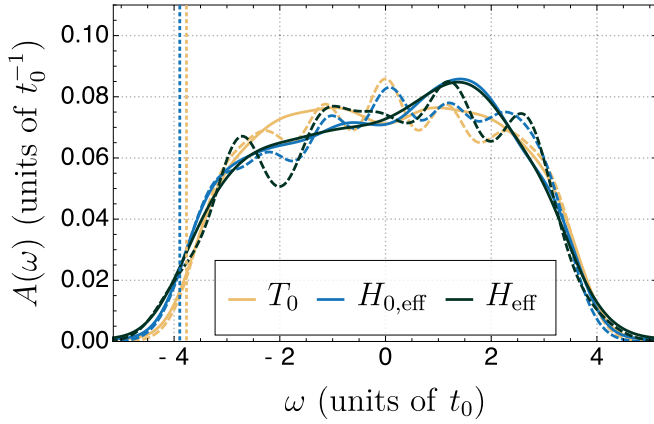


FIG. 10. Spectral densities $A(\omega)$ for the square lattice, parameter set (A), and the various contributions, calculated with CET for $N = 18$ (solid) and iEoM for $m = 4$ for T_0 and $H_{0,\text{eff}}$ and $m = 3$ for H_{eff} (dashed). All data are convolved with $\sigma = 0.45t_0$. The band edges ω_{min} calculated according to (37) are indicated by vertical dashed lines.

powers of t . The result reads

$$g(t) \approx -\frac{i}{2}(1 + \langle [H, \bar{h}_{i,\uparrow}(0)][H, \bar{h}_{i,\uparrow}^\dagger(0)] \rangle t^2) + O(t^3), \quad (\text{A1})$$

where the translational invariance in time, i.e.,

$$g'(t) = g'(-t) = \langle [H, \bar{h}_{i,\uparrow}(0)]\bar{h}_{i,\uparrow}^\dagger(-t) \rangle, \quad (\text{A2})$$

allows us to apply the second derivative to the second operator,

$$g''(t) = \frac{dg'(-t)}{dt} = -i\langle [H, \bar{h}_{i,\uparrow}(0)][H, \bar{h}_{i,\uparrow}^\dagger(0)] \rangle. \quad (\text{A3})$$

In this way, a double commutator is avoided.

For clarity, we apply formula (A1) to the one-dimensional chain. The commutators appearing are

$$[T_0, \bar{h}_{i,\uparrow}] = t_0\bar{h}_{i\pm 1,\downarrow}\sigma_i^+ + \frac{1}{2}t_0\bar{h}_{i\pm 1,\uparrow}\sigma_i^z + \frac{1}{2}t_0\bar{h}_{i\pm 1,\uparrow}, \quad (\text{A4a})$$

$$[T_0'', \bar{h}_{i,\uparrow}] = t''\bar{h}_{i\pm 2,\downarrow}\sigma_i^+ + \frac{1}{2}t''\bar{h}_{i\pm 2,\uparrow}\sigma_i^z + \frac{1}{2}t''\bar{h}_{i\pm 2,\uparrow}, \quad (\text{A4b})$$

$$[T_{s,0}'', \bar{h}_{i,\uparrow}] = \frac{1}{2}t_s''\bar{h}_{i\pm 2,\downarrow}\sigma_{i\pm 1}^+ + \frac{1}{2}t_s''\bar{h}_{i\pm 2,\downarrow}\sigma_{i\pm 1}^z \quad (\text{A4c})$$

$$+ t_s''\bar{h}_{i\pm 2,\uparrow}\sigma_{i\pm 1}^- + \frac{1}{4}t_s''\bar{h}_{i\pm 2,\uparrow}\sigma_{i\pm 1}^z \quad (\text{A4d})$$

$$+ \frac{1}{4}t_s''\bar{h}_{i\pm 2,\uparrow}\sigma_{i\pm 1}^z\sigma_i^z - \frac{1}{2}t_s''\bar{h}_{i\pm 2,\downarrow}\sigma_{i\pm 1}^z\sigma_i^+, \quad (\text{A4e})$$

$$[H_J, \bar{h}_{i,\uparrow}] = \frac{1}{4}J\bar{h}_{i,\uparrow}\sigma_{i\pm 1}^z + \frac{1}{2}\bar{h}_{i,\downarrow}\sigma_{i\pm 1}^+. \quad (\text{A4f})$$

The remaining commutators for the case $\bar{h}_{i,\uparrow}^\dagger$ result from the relations (A4) substituting $\bar{h}_{i,\uparrow} \rightarrow -\bar{h}_{i,\uparrow}^\dagger$ as well as $\sigma^+ \leftrightarrow \sigma^-$. The expectation values occurring in (A1) can be calculated straightforwardly since they are to be determined at $t = 0$. The trace is computed over states at half-filling without a hole. For demonstration purposes, we give the results for the

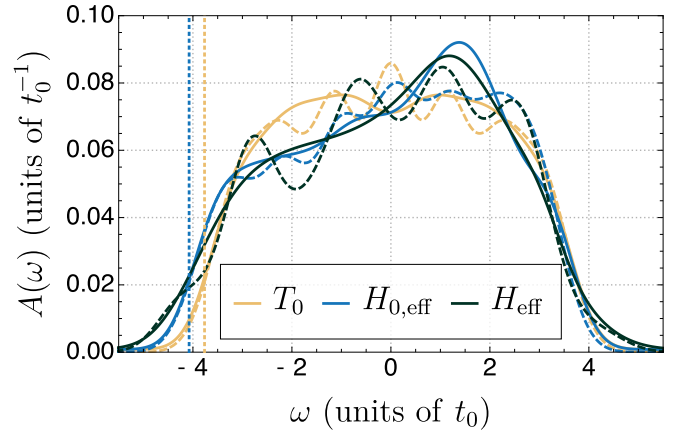


FIG. 11. Same as in Fig. 10, but for parameter set (B).

expectation values that arise from H_J [see (A4f)],

$$\langle \bar{h}_{i,\uparrow}\sigma_{i\pm 1}^z\bar{h}_{i,\uparrow}^\dagger\sigma_{i\pm 1}^z \rangle = 2 \times \frac{1}{2}, \quad (\text{A5a})$$

$$\langle \bar{h}_{i,\downarrow}\sigma_{i\pm 1}^+\bar{h}_{i,\downarrow}^\dagger\sigma_{i\pm 1}^- \rangle = 2 \times \frac{1}{4}. \quad (\text{A5b})$$

Here, the first factor results from the double occurrence of the expectation value, once for $i + 1$ and once for $i - 1$. The expectation values from the other contributions can be calculated similarly. Substituting all expectation values and (A4) into (A1) then yields the explicit expansion

$$g(t) = -\frac{i}{2}\left[1 - \left(t_0^2 + t''^2 + \frac{6}{16}t_s''^2 + \frac{3}{32}J^2\right)t^2\right] + O(t^3). \quad (\text{A6})$$

APPENDIX B: 2D RESULTS FROM IEOM AND CET

In addition to the results obtained for the square lattice using CET, convolved with $\sigma = 0.15t_0$, and shown in Figs. 8 and 9, the analogous results can also be obtained using iEoM. Due to the limited loop order m they need to be broadened more strongly by Gaussians.

Due to the limited maximum loop order m , wiggly spectral densities occur. To ensure a reasonable comparability to CET results and to show the good agreement of both methods, a convolution of (all) results with an increased $\sigma = 0.45t_0$ is performed. Still, the iEoM results display some spurious wiggles. The corresponding results for the sets (A) and (B) are depicted in Figs. 10 and 11. The increased width of the CET results compared to the ones in Figs. 8 and 9 is an artefact due to the enhanced broadening. Obviously, the band edges obtained from the minimum eigenvalues of the Liouville matrix in iEoM are identical regardless of the additional broadening. Increasing the loop order m is likely to lead to a higher similarity of the results of both methods.

- [1] F. Gebhard, *The Mott Metal-Insulator Transition*, Springer Tracts in Modern Physics Vol. 137 (Springer, Berlin, 1997).
 [2] J. G. Bednorz and K. A. Müller, Possible high- t_c superconductivity, *Z. Phys. B* **64**, 189 (1986).

- [3] P. W. Anderson, The resonating valence bond state in La_2CuO_4 and superconductivity, *Science* **235**, 1196 (1987).
 [4] W. F. Brinkman and T. M. Rice, Single-particle excitations in magnetic insulators, *Phys. Rev. B* **2**, 1324 (1970).

- [5] S. A. Trugman, Interaction of holes in a Hubbard antiferromagnet and high-temperature superconductivity, *Phys. Rev. B* **37**, 1597 (1988).
- [6] S. Schmitt-Rink, C. M. Varma, and A. E. Ruckenstein, Spectral Function of Holes in a Quantum Antiferromagnet, *Phys. Rev. Lett.* **60**, 2793 (1988).
- [7] C. L. Kane, P. A. Lee, and N. Read, Motion of a single hole in a quantum antiferromagnet, *Phys. Rev. B* **39**, 6880 (1989).
- [8] Z. Liu and E. Manousakis, Dynamical properties of a hole in a Heisenberg antiferromagnet, *Phys. Rev. B* **45**, 2425 (1992).
- [9] W. Metzner, P. Schmit, and D. Vollhardt, Hole dynamics in a spin background: A sum-rule conserving theory with exact limits, *Phys. Rev. B* **45**, 2237 (1992).
- [10] A. Belkasi and J. L. Richard, Motion of a single hole in a disordered magnetic background, *Phys. Lett. A* **197**, 353 (1995).
- [11] K. A. Hallberg, E. Müller-Hartmann, and C. A. Balseiro, Hole dynamics in generalized spin backgrounds in infinite dimensions, *Phys. Rev. B* **52**, 4396 (1995).
- [12] M. Vojta and K. W. Becker, Hole motion in an arbitrary spin background: Beyond the minimal spin-polaron approximation, *Phys. Rev. B* **57**, 3099 (1998).
- [13] J. Bonča, S. Maekawa, and T. Tohyama, Numerical approach to the low-doping regime of the t - J model, *Phys. Rev. B* **76**, 035121 (2007).
- [14] A. Nocera, F. H. L. Essler, and A. E. Feiguin, Finite-temperature dynamics of the Mott insulating Hubbard chain, *Phys. Rev. B* **97**, 045146 (2018).
- [15] M. Mierzejewski, L. Vidmar, J. Bonča, and P. Prelovšek, Nonequilibrium Quantum Dynamics of a Charge Carrier Doped Into a Mott Insulator, *Phys. Rev. Lett.* **106**, 196401 (2011).
- [16] J. Vijayan, P. Sompet, G. Salomon, J. Koepsell, S. Hirthe, A. Bohrdt, F. Grusdt, I. Bloch, and C. Gross, Time-resolved observation of spin-charge deconfinement in fermionic hubbard chains, *Science* **367**, 186 (2020).
- [17] G. Ji, M. Xu, L. H. Kendrick, C. S. Chiu, J. C. Brüggjenjürgen, D. Greif, A. Bohrdt, F. Grusdt, E. Demler, M. Lebrat, and M. Greiner, Coupling a Mobile Hole to an Antiferromagnetic Spin Background: Transient Dynamics of a Magnetic Polaron, *Phys. Rev. X* **11**, 021022 (2021).
- [18] F. Grusdt, M. Kánasz-Nagy, A. Bohrdt, C. S. Chiu, G. Ji, M. Greiner, D. Greif, and E. Demler, Parton Theory of Magnetic Polarons: Mesonic Resonances and Signatures in Dynamics, *Phys. Rev. X* **8**, 011046 (2018).
- [19] A. Bohrdt, E. Demler, F. Pollmann, M. Knap, and F. Grusdt, Parton theory of angle-resolved photoemission spectroscopy spectra in antiferromagnetic Mott insulators, *Phys. Rev. B* **102**, 035139 (2020).
- [20] A. Bohrdt, F. Grusdt, and M. Knap, Dynamical formation of a magnetic polaron in a two-dimensional quantum antiferromagnet, *New J. Phys.* **22**, 123023 (2020).
- [21] A. Mielke, The one-dimensional Hubbard model for large or infinite U , *J. Stat. Phys.* **62**, 509 (1991).
- [22] B. Kumar, Exact solution of the infinite- U Hubbard problem and other models in one dimension, *Phys. Rev. B* **79**, 155121 (2009).
- [23] M. P. Eastwood, F. Gebhard, E. Kalinowski, S. Nishimoto, and R. M. Noack, Analytical and numerical treatment of the Mott-Hubbard insulator in infinite dimensions, *Eur. Phys. J. B* **35**, 155 (2003).
- [24] S. Nishimoto, F. Gebhard, and E. Jeckelmann, Dynamical density-matrix renormalization group for the Mott-Hubbard insulator in high dimensions, *J. Phys.: Condens. Matter* **16**, 7063 (2004).
- [25] R. Bulla, Zero Temperature Metal-Insulator Transition in the Infinite-Dimensional Hubbard Model, *Phys. Rev. Lett.* **83**, 136 (1999).
- [26] R. Bulla, T. A. Costi, and D. Vollhardt, Finite temperature numerical renormalization group study of the Mott-transition, *Phys. Rev. B* **64**, 045103 (2001).
- [27] D. J. Garcia, K. Hallberg, and M. J. Rozenberg, Dynamical Mean Field Theory with the Density Matrix Renormalization Group, *Phys. Rev. Lett.* **93**, 246403 (2004).
- [28] N. Blümer and E. Kalinowski, The Mott insulator: Tenth-order perturbation theory extended to infinite order using a quantum Monte Carlo, *Phys. Rev. B* **71**, 195102 (2005).
- [29] M. Karski, C. Raas, and G. S. Uhrig, Electron spectra close to a metal-to-insulator transition, *Phys. Rev. B* **72**, 113110 (2005).
- [30] M. Karski, C. Raas, and G. S. Uhrig, Single-particle dynamics in the vicinity of the Mott-Hubbard metal-to-insulator transition, *Phys. Rev. B* **77**, 075116 (2008).
- [31] J. Carlström, N. Prokof'ev, and B. Svistunov, Quantum Walk in Degenerate Spin Environments, *Phys. Rev. Lett.* **116**, 247202 (2016).
- [32] M. Kanász-Nagy, I. Lovas, F. Grusdt, D. Greif, M. Greiner, and E. A. Demler, Quantum correlations at infinite temperature: The dynamical Nagaoka effect, *Phys. Rev. B* **96**, 014303 (2017).
- [33] F. H. L. Essler, H. Frahm, F. Göhmann, A. Klümper, and V. E. Korepin, *The One-Dimensional Hubbard Model* (Cambridge University Press, Cambridge, UK, 2005).
- [34] S. Ejima, F. H. Essler, and F. Gebhard, Thermodynamics of the one-dimensional half-filled Hubbard model in the spin-disordered regime, *J. Phys. A* **39**, 4845 (2006).
- [35] P. W. Anderson, New approach to the theory of superexchange interactions, *Phys. Rev.* **115**, 2 (1959).
- [36] A. B. Harris and R. V. Lange, Single-particle excitations in narrow energy bands, *Phys. Rev.* **157**, 295 (1967).
- [37] D. J. Klein and W. A. Seitz, Perturbation expansion of the linear Hubbard model, *Phys. Rev. B* **8**, 2236 (1973).
- [38] M. Takahashi, Half-filled Hubbard model at low temperature, *J. Phys. C* **10**, 1289 (1977).
- [39] A. H. MacDonald, S. M. Girvin, and D. Yoshioka, t/U expansion for the Hubbard model, *Phys. Rev. B* **37**, 9753 (1988).
- [40] J. Stein, Flow equations and the strong-coupling expansion for the Hubbard model, *J. Stat. Phys.* **88**, 487 (1997).
- [41] H. Eskes, A. M. Oleś, M. B. J. Meinders, and W. Stephan, Spectral properties of the Hubbard bands, *Phys. Rev. B* **50**, 17980 (1994).
- [42] A. Reischl, E. Müller-Hartmann, and G. S. Uhrig, Systematic mapping of the Hubbard model to the generalized t - J model, *Phys. Rev. B* **70**, 245124 (2004).
- [43] S. A. Hamerla, S. Duffe, and G. S. Uhrig, Derivation of the t - J model for finite doping, *Phys. Rev. B* **82**, 235117 (2010).
- [44] M. Kalthoff, F. Keim, H. Krull, and G. S. Uhrig, Comparison of the iterated equation of motion approach and the density matrix formalism for the quantum Rabi model, *Eur. Phys. J. B* **90**, 97 (2017).
- [45] P. Bleicker and G. S. Uhrig, Strong quenches in the one-dimensional Fermi-Hubbard model, *Phys. Rev. A* **98**, 033602 (2018).

- [46] H. Tal-Ezer and R. Kosloff, An accurate and efficient scheme for propagating the time dependent Schrödinger equation, *J. Chem. Phys.* **81**, 3967 (1984).
- [47] A. Weiße, G. Wellein, A. Alvermann, and H. Fehske, The kernel polynomial method, *Rev. Mod. Phys.* **78**, 275 (2006).
- [48] P. Bleicker, J. Stolze, and G. S. Uhrig, Probing thermalization in quenched integrable and nonintegrable Fermi-Hubbard models, *Phys. Rev. A* **102**, 013321 (2020).
- [49] J. Hubbard, Electron correlations in narrow energy bands, *Proc. Roy. Soc. Lond.* **276**, 238 (1963).
- [50] J. Kanamori, Electron correlation and ferromagnetism of transition metals, *Prog. Theor. Phys.* **30**, 275 (1963).
- [51] M. C. Gutzwiller, Effect of correlation on the ferromagnetism of transition metals, *Phys. Rev.* **134**, A923 (1964).
- [52] A. Mielke, Flow equations for band-matrices, *Eur. Phys. J. B* **5**, 605 (1998).
- [53] C. Knetter and G. S. Uhrig, Perturbation theory by flow equations: dimerized and frustrated $s = 1/2$ chain, *Eur. Phys. J. B* **13**, 209 (2000).
- [54] S. Kehrein, *The Flow Equation Approach to Many-Particle Systems*, Springer Tracts in Modern Physics Vol. 217 (Springer, Berlin, 2006).
- [55] G. S. Uhrig, Interaction quenches of Fermi gases, *Phys. Rev. A* **80**, 061602(R) (2009).
- [56] S. A. Hamerla and G. S. Uhrig, Dynamical transition in interaction quenches of the one-dimensional Hubbard model, *Phys. Rev. B* **87**, 064304 (2013).
- [57] S. A. Hamerla and G. S. Uhrig, Interaction quenches in the two-dimensional fermionic Hubbard model, *Phys. Rev. B* **89**, 104301 (2014).
- [58] C. Lanczos, An iteration method for the solution of the eigenvalue problem of linear differential and integral operators, *J. Res. Natl. Bur. Stand.* **45**, 255 (1950).
- [59] J. Skilling, *Maximum Entropy and Bayesian Methods*, edited by J. Skilling (Springer, Dordrecht, 1988), pp. 455–466.
- [60] D. A. Drabold and O. F. Sankey, Maximum Entropy Approach for Linear Scaling in the Electronic Structure Problem, *Phys. Rev. Lett.* **70**, 3631 (1993).
- [61] R. Silver and H. Röder, Densities of states of mega-dimensional Hamiltonian matrices, *Int. J. Mod. Phys. C* **05**, 735 (1994).